JACS
JOURNAL OF THE AMERICAN CHEMICAL SOCIETY

Communication

pubs.acs.org/JACS

Photoelectrochemical Oxidation of Water Using $BaTaO_2N$ Photoanodes Prepared by Particle Transfer Method

Koichiro Ueda,[†] Tsutomu Minegishi,[†] Justin Clune,[†] Mamiko Nakabayashi,[§] Takashi Hisatomi,[†] Hiroshi Nishiyama,[‡] Masao Katayama,[‡] Naoya Shibata,[§] Jun Kubota,[†] Taro Yamada,[‡] and Kazunari Domen*,[†]

[†]Department of Chemical System Engineering, School of Engineering, The University of Tokyo, 7-3-1 Hongo, Bunkyo-ku, Tokyo 113-8656, Japan

[‡]Department of Chemical System Engineering, School of Engineering, The University of Tokyo, 5-1-5 Kashiwanoha, Kashiwa, Chiba 277-8589, Japan

[§]Institute of Engineering Innovation, The University of Tokyo, 2-11-16 Yayoi, Bunkyo-ku, Tokyo 113-8656, Japan

Supporting Information

ABSTRACT: A photoanode of particulate $BaTaO_2N$ fabricated by the particle transfer method and modified with a Co cocatalyst generated a photocurrent of 4.2 mA cm^{-2} at 1.2 V_{RHE} in the photoelectrochemical water oxidation reaction under simulated sunlight (AM1.5G). The half-cell solar-to-hydrogen conversion efficiency (HC-STH) of the photoanode reached 0.7% at 1.0 V_{RHE}, which was an order of magnitude higher than the previously reported photoanode made from the same material. The faradaic efficiency for oxygen evolution from water was virtually 100% during the reaction for 6 h, attesting to the robustness of the oxynitride.

Fossil resources such as petroleum oil, natural gas, and coal are used as essential fuels in human society and as raw materials for bulk chemicals such as hydrogen, methanol, and ammonia. However, these resources will eventually be depleted and replacement of fossil fuels by renewable energy resources is needed. Photoelectrochemical (PEC) water splitting, which can produce hydrogen and oxygen directly from solar irradiation,[1] as well as photocatalytic water splitting,[2,3] is a possible means of producing hydrogen in an environmentally friendly manner. For efficient solar energy conversion, a photoelectrode should satisfy at least three requirements: an appropriate band gap for sunlight absorption, a suitable band structure for water reduction/oxidation, and durability under the reaction conditions.

Oxynitride semiconducting materials (e.g., ZnO:GaN,[3] TaON,[4] $LaTiO_2N$,[5] etc.) have received considerable attention due to their suitable properties as photocatalysts and photoelectrodes for water splitting. Among them, $BaTaO_2N$ (BTON) is one of the most promising candidates as a photoanode for oxygen evolution from water because of its band gap, which is narrow enough to absorb visible light up to 660 nm while straddling the potentials of the hydrogen and oxygen evolution reactions.[6,7] This ideal band structure is due to the shallow potential of the valence band maximum, which is composed of hybridized N 2p and O 2p orbitals.[8] Assuming incident photon-to-current conversion efficiency (IPCE) values of 100% in the wavelength region of <660 nm, a BTON photoanode could generate a photocurrent of ~18 mA cm^{-2} under AM1.5G light. Higashi et al. demonstrated stable oxygen evolution from water for over 1 h and the utilization of relatively long wavelength light (>600 nm) using BTON photoanodes fabricated by electrophoretic deposition with surface modifications,[7] although the photocurrent was significantly lower than the theoretical upper limit, even under intense illumination from a 300 W Xe lamp.

In the present study, the PEC properties of BTON photoanodes fabricated using the particle transfer method were investigated.[9,10] A photoanode modified with Co species showed stable oxygen evolution from water for 6 h with a faradaic efficiency of unity under simulated AM1.5G light. Under the visible light from a 300 W Xe lamp equipped with filters, the photocurrent at an applied potential of 1.2 V_{RHE} reached 25 mA cm^{-2}, ~10 times higher that of previously reported BTON photoanodes.[7]

The oxide precursors were prepared by a conventional solid state reaction. A mixture of $BaCO_3$ and Ta_2O_5 powders was calcined in air at 1273 K for 10 h, resulting in the formation of $Ba_5Ta_4O_{15}$ powder. (See Figure S1a in the Supporting Information (SI).) A BTON photocatalyst powder was obtained by nitriding the oxide precursor at 1173 K for 30 h under an NH_3 flow of 250 mL min^{-1}. X-ray diffraction results indicated that no obvious impurity was formed in the prepared BTON powder, as shown in Figure S2 in the SI. Photoelectrodes were fabricated from the BTON powder by the particle transfer method described in previous reports.[9,10] Briefly, 50 mg of BTON were dispersed in 1 mL of methanol by sonication for 30 min. The suspension was dropped onto a 30 × 30 mm^2 quartz glass plate to form layers of BTON particles. After drying the solvent, a Ta metal contact layer and a Ti metal conductor layer were deposited on the BTON particle layer using radio frequency (RF) magnetron sputtering. The Ti conductor layer was deposited at 423 K, while the Ta contact layer was deposited at various temperatures from 423 to 1023 K. Subsequently, the assembly of BTON particles and Ta/Ti metal films (BTON/Ta/Ti) was peeled from the glass plate and sonicated in distilled water to wash off excess particles that were loosely attached to the

Received: December 27, 2014
Published: February 4, 2015

DOI: 10.1021/ja5131879
J. Am. Chem. Soc. 2015, 137, 2227−2230

BTON/Ta/Ti assembly. Then, the assembly was fixed onto a glass plate using carbon tape, and the metal layer was connected to a copper wire using indium solder. The unnecessary surface was covered with epoxy resin. A three-electrode system was used in PEC experiments and depositions of Co species using a potentiostat (HSV-120, Hokuto). Prior to the PEC measurements, a Co cocatalyst was deposited on the BTON/Ta/Ti photoanodes by electrodeposition at 1.7 V_{RHE} for 100 s in aqueous solutions of 20 mM $Co(NO_3)\cdot 6H_2O$, 0.1 M K_2HPO_4, and 0.1 M KH_2PO_4.[11] The prepared samples were characterized using X-ray diffraction (XRD; RINT-Ultima3, Rigaku), UV–visible diffuse reflection spectroscopy (UV–vis DRS; V-670DS, JUSCO), scanning electron microscopy (SEM; S-4800, Hitachi), and transmission electron microscopy (TEM; JEM-2800, JEOL). The detailed characterization of the samples is presented in the SI.

Figure 1 shows SEM images of a BTON/Ta/Ti electrode. The Ta contact layer was deposited at 873 K. In the top-view images,

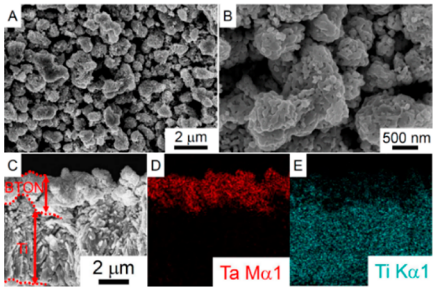

Figure 1. Top view (A, B) and cross-sectional SEM images (C) of a BTON/Ta/Ti electrode, along with simultaneously measured EDX mappings (D, E). The Ta contact layer was deposited at 873 K.

micrometer-sized porous particles of BTON were observed on the surface of the electrode. The cross-sectional observation revealed that the average thickness of the BTON particle layer was about 2 μm, which is comparable to the secondary particle size of the BTON. For closer examination of the electrode structure, high resolution TEM observation was conducted. The scanning transmission electron microscopy (STEM) images and simultaneously measured EDX mapping shown in Figure 2A–D revealed that a 70-nm-thick Ta contact layer, which appeared as a bright layer between the BTON particles and the thicker Ti

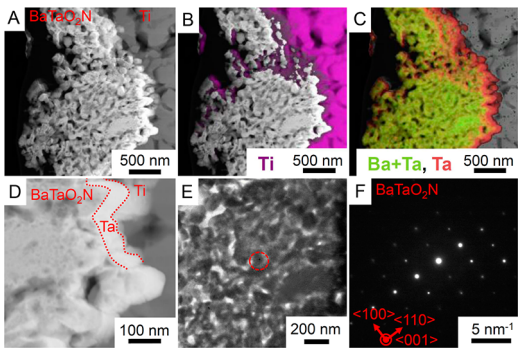

Figure 2. Cross-sectional TEM images of a BTON/Ta/Ti electrode: STEM dark field image of BTON/Ta/Ti interfaces with low magnifications (A) and simultaneously measured EDX mapping results (B, C), STEM dark field image of BTON/Ta/Ti interfaces with high magnifications (D), a TEM image of BTON particles (E), and a selected area diffraction pattern (SADP) of the circled region in Figure 2C (F).

conductor layer, was connected with the BTON particles. Such uniform and dense contact between semiconductor particles and metal layers is beneficial for charge transfer, because carrier transport through the BTON particle layers would not be efficient due to the high electrical resistivity within the semiconductor and at the grain boundaries. As shown in Figure 2E, primary particles ~100 nm in size were in intimate contact with each other. The selected area diffraction pattern (SADP) of the circled region in Figure 2E is shown in Figure 2F. It is possible to assign the zone axis as BTON ⟨001⟩. The crystal directions of ⟨100⟩ and ⟨110⟩ can also be identified from the spacing between the diffraction spots, as illustrated in Figure 2F. Therefore, we conclude that the primary particles of the porous secondary particles are single-crystalline BTON.

A current potential (I–E) curve of a Co-modified BTON/Ta/Ti (Co/BTON/Ta/Ti) electrode under simulated AM1.5G light is shown in Figure 3. The anodic photocurrent increased

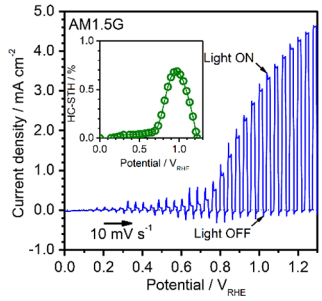

Figure 3. I–E curve of a Co/BTON/Ta/Ti photoelectrode under simulated AM1.5G light. A 0.2 M potassium phosphate aqueous solution adjusted to pH 13 by adding KOH was used as an electrolyte. The applied potential was swept at +10 mV s^{-1} under intermittent irradiation with a period of 2 s.

significantly at 0.7 V_{RHE} and above, reaching 4.2 mA cm^{-2} at 1.2 V_{RHE}. An anodic photoresponse was observed at potentials below 0.2 V_{RHE}, which was indicative of a preferable band structure for PEC oxygen evolution from water. The flat band potential below 0 V_{RHE}, as determined from Mott–Schottky (MS) plots (Figure S8 in the SI), also supports the potential of BTON as a photoanode. The half-cell solar-to-hydrogen conversion efficiency (HC-STH) reached 0.7% at 1.0 V_{RHE}, as shown in the inset of Figure 3. I–E curves of Co/BTON/Ta/Ti photoanodes with Ta deposition temperatures lower than 773 K generated lower photocurrents (see Figure S6 in the SI). The optimum deposition temperature of the Ta contact layers was thus determined to be 873 K. To clarify the impact of the Ta deposition temperature, electrochemical impedance spectroscopy was conducted. BTON/Ta/Ti photoanodes prepared with higher Ta deposition temperatures had higher slopes in their MS plots, as shown in Figure S8 in the SI. Note that a higher slope in the MS plot should indicate lower electron donor concentrations and a wider depletion layer if the morphologies of the electrodes are comparable. Accordingly, higher Ta deposition temperatures increased the electrical resistivity of the BTON particles. The optimum temperature of Ta deposition was most likely determined by the electrical resistivity that balanced the depletion layer thickness at the solid–liquid interface and the series resistance within the BTON particle layers. Furthermore, removal of contaminants from the surfaces of the BTON particles is another possible reason for the photocurrent increase at higher Ta deposition temperatures.

DOI: 10.1021/ja5131879
J. Am. Chem. Soc. 2015, 137, 2227–2230

The IPCE values were measured from constant potential $I-t$ curve measurements obtained under continuous monochromatic light irradiation to avoid the transient photoresponse. Figure 4

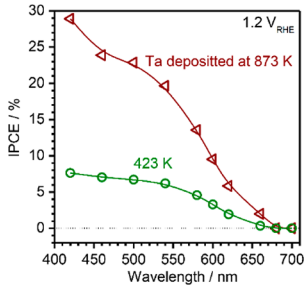

Figure 4. Wavelength dependence of IPCE for Co/BTON/Ta/Ti electrodes. The Ta layers were deposited at 423 and 873 K. The IPCE values were measured from a constant potential $I-t$ curve at 1.2 V_{RHE} in 0.2 M potassium phosphate aqueous solution (pH 13) under monochromatic light with a wavelength width of 20 nm. The light intensity was $(2-3) \times 10^{16}$ photons cm^{-2} s^{-1}.

shows the wavelength dependence of the IPCE of Co/BTON/Ta/Ti electrodes with Ta contact layers deposited at 423 and 873 K. For both Ta deposition temperatures, the IPCE at an applied potential of 1.2 V_{RHE} became zero at 700 nm, which is near the absorption edge of BTON. The Co/BTON/Ta/Ti with a Ta deposition temperature of 873 K had 3−4 times higher IPCEs at wavelengths of <660 nm than the sample with a Ta deposition temperature of 423 K, and there was no significant difference in the spectral shapes of the IPCEs. The IPCEs are consistent with $I-E$ curves measured under simulated AM1.5G light, supporting the validity of the measurements. Under a photon flux equivalent to the AM1.5G solar spectrum with wavelengths less than 660 nm, the present Co/BTON/Ta/Ti electrode showed higher IPCEs than the reported values, especially at <540 nm under an applied potential of 1.2 V_{RHE}.[7] To enhance the IPCEs at wavelengths longer than 540 nm, a thicker depletion layer and a longer diffusion length for holes are desirable, considering the deeper penetration longer wavelength light.

Gas product analysis was conducted to confirm the faradaic efficiency. Figure 5A shows an $I-t$ curve of a Co/BTON/Ta/Ti electrode at 0.8 V_{RHE} under simulated AM1.5G light. It should be noted that a CrO_x-coated Pt mesh was used as a counter electrode to avoid reverse reactions on the Pt surfaces. The potential of the counter electrode was constant at approximately −0.05 V_{RHE}, indicating that the applied bias voltage between the

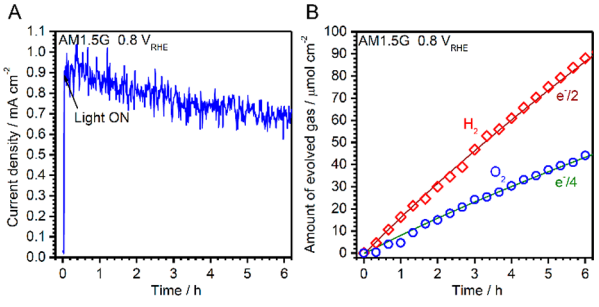

Figure 5. $I-t$ curve of a Co/BTON/Ta/Ti electrode at 0.8 V_{RHE} under simulated AM1.5G light (A) and simultaneously measured amounts of evolved hydrogen and oxygen (b). A 0.2 M potassium phosphate aqueous solution (pH 13) and a CrO_x-coated Pt mesh were used as the electrolyte and counter electrode, respectively.

photoanode and the counter electrode was ∼0.85 V throughout the measurement (see Figure S9 in the SI). The amounts of evolved hydrogen and oxygen are plotted in Figure 5B. The estimated amounts of the gases based on the passed current and a faradaic efficiency of unity are also shown, with solid curves labeled $e^-/2$ and $e^-/4$ for hydrogen and oxygen, respectively. The photocurrent was almost constant for ∼1 h, although some fluctuation was observed due to bubble formation on the electrode surfaces. The photocurrent decreased gradually by 20% over 6 h, while the faradaic efficiency of virtually 100% was maintained throughout the measurement. Therefore, BTON was considered to be sufficiently stable during PEC water oxidation. The decrease in photocurrent should be attributed to other factors, such as detachment of the amorphous Co catalyst because of oxidation by photoexcited holes, rather than to degradation of the oxynitride. The HC-STH, estimated from the $I-t$ curve, was 0.5% for the initial current of 0.9 mA cm^{-2} and 0.4% for the photocurrent after 6 h of 0.7 mA cm^{-2}.

To evaluate the photocurrent under higher intensity light, and to compare it with previous reports, the photoresponse of the Co/BTON/Ta/Ti photoanode was measured under illumination by a 300 W Xe lamp (∼13 times the sun's intensity) at wavelengths of <660 nm (see Figure S7 in the SI). An $I-E$ curve for a Co/BTON/Ta/Ti electrode under visible light (>420 nm) irradiation from a 300 W Xe lamp equipped with filters is shown in Figure S10 in the SI. An anodic photoresponse was observed below 0.1 V_{RHE}. The photocurrent increased significantly at 0.5 V_{RHE} and above. The photocurrent at an applied potential of 1.2 V_{RHE} reached 25 mA cm^{-2}, ∼10 times that of the previously reported BTON photoanodes.[7]

In summary, a photoanode of particulate BTON fabricated by the particle transfer method using a Ta contact layer, a Ti conductor layer, and a Co cocatalyst generated an anodic photocurrent of 4.2 mA cm^{-2} at 1.2 V_{RHE}, and the anodic photocurrent increased significantly at 0.7 V_{RHE} and above under simulated AM1.5G light. An anodic photoresponse was observed at potentials below 0.2 V_{RHE} because of the favorable band structure of BTON. The optimal deposition temperature of the Ta contact layer was 873 K because the appropriate electrical resistivity of the BTON particles enabled adequate charge separation at the solid−liquid interface and electrical conduction within the BTON particle layers. The photoanodic current of the Co/BTON/Ta/Ti gradually decreased by 20% over 6 h at 0.8 V_{RHE} under simulated AM1.5G light. However, the faradaic efficiency of 100% was maintained throughout the $I-t$ measurement. HC-STH was 0.5% for an initial current of 0.9 mA cm^{-2}. Under irradiation from a 300 W Xe lamp equipped with filters, the photocurrent at an applied potential of 1.2 V_{RHE} reached 25 mA cm^{-2}. This is ∼10 times that of the previous report.[7] Throughout the investigation, the possibility of efficient and durable water oxidation under sunlight using particle-based BTON photoanodes was confirmed. However, there remains considerable room to improve the photocurrent and to stabilize the electrode surface.[9,12,13] The photocurrent should be increased by surface modification with a p-type material to form a p−n junction on the photoanode surface, as in the case of photocathodes.[12] The durability of the BTON photoanodes may be improved by surface coating with thin oxides by atomic layer deposition or other techniques.

DOI: 10.1021/ja5131879
J. Am. Chem. Soc. 2015, 137, 2227−2230

■ ASSOCIATED CONTENT

Supporting Information

The results of sample analysis, *I*−*E* curves for Co/BTON/Ta/Ti electrodes prepared with various Ta deposition temperatures, spectra of the light sources, MS plots for BTON/Ta/Ti electrodes, the potential of the counter electrode during the *I*−*t* measurement, an *I*−*E* curve of Co/BTON/Ta/Ti under a 300 W Xe lamp equipped with filters, and the deposition conditions of Ta contact layers and Ti conductor layers. This material is available free of charge via the Internet at http://pubs.acs.org.

■ AUTHOR INFORMATION

Corresponding Author

*domen@chemsys.t.u-tokyo.ac.jp

Notes

The authors declare no competing financial interest.

■ ACKNOWLEDGMENTS

Advice and comments by Prof. Yuichi Ikuhara have been a great help in the structural characterization. This work was partly supported by the Artificial Photosynthesis Project of the Ministry of Economy, Trade and Industry (METI) of Japan. This work was also supported in part by a Grant-in-Aid for Specially Promoted Research (#23000009) and the international exchange program of the A3 Foresight Program of the Japan Society for the Promotion of Science (JSPS). M.N. and N.S. acknowledge financial support by "Nanotechnology Platform" (project No.12024046) from MEXT of Japan.

■ REFERENCES

(1) Lewis, N. S. *Science* **2007**, *315*, 798−801. Lewis, N. S.; Nocera, D. G. *Proc. Natl. Acad. Sci. U.S.A.* **2006**, *103*, 15729−15735. Pinaud, B. A.; Benck, J. D.; Seitz, L. C.; Forman, A. J.; Chen, Z.; Deutsch, T. G.; James, B. D.; Baum, K. N.; Baum, G. N.; Ardo, S.; Wang, H.; Miller, E.; Jaramillo, T. F. *Energy Environ. Sci.* **2013**, *6*, 1983−2002.

(2) Sato, S.; White, J. M. *Chem. Phys. Lett.* **1980**, *72*, 83−86. Domen, K.; Naito, S.; Soma, M.; Onishi, T.; Tamaru, K. *J. Chem. Soc., Chem. Commun.* **1980**, 543−544. Kato, H.; Asakura, K.; Kudo, A. *J. Am. Chem. Soc.* **2003**, *125*, 3082−3089. Sakata, Y.; Matsuda, Y.; Nakagawa, T.; Yasunaga, R.; Imamura, H.; Teramura, K. *ChemSusChem* **2011**, *4*, 181−184. Kudo, A.; Miseki, Y. *Chem. Soc. Rev.* **2009**, *38*, 253−278. Abe, R. *J. Photochem. Photobiol., C* **2010**, *11*, 179−209. Hisatomi, T.; Kubota, J.; Domen, K. *Chem. Soc. Rev.* **2014**, *43*, 7520−7535.

(3) Maeda, K.; Domen, K. *J. Phys. Chem. Lett.* **2010**, *1*, 2655−2661. Maeda, K.; Domen, K. *J. Phys. Chem. C* **2007**, *111*, 7851−7861.

(4) Hitoki, G.; Takata, T.; Kondo, J. N.; Hara, M.; Kobayashi, H.; Domen, K. *Chem. Commun.* **2002**, 1698−1699.

(5) Kasahara, A.; Nukumizu, K.; Takata, T.; Kondo, J. N.; Hara, M.; Kobayashi, H.; Domen, K. *J. Phys. Chem. B* **2003**, *107*, 791−797. Kasahara, A.; Nukumizu, K.; Hitoki, G.; Takata, T.; Kondo, J. N.; Hara, M.; Kobayashi, H.; Domen, K. *J. Phys. Chem. A* **2002**, *106*, 6750−6753.

(6) Higashi, M.; Abe, R.; Teramura, K.; Takata, T.; Ohtani, B.; Domen, K. *Chem. Phys. Lett.* **2008**, *452*, 120−123. Higashi, M.; Abe, R.; Takata, T.; Domen, K. *Chem. Mater.* **2009**, *21*, 1543−1549. Matoba, T.; Maeda, K.; Domen, K. *Chem.—Eur. J.* **2011**, *17*, 14731−14735. Maeda, K.; Domen, K. *Angew. Chem., Int. Ed.* **2012**, *51*, 9865−9869. Maeda, K.; Lu, D.; Domen, K. *Angew. Chem., Int. Ed.* **2013**, *52*, 6488−6491. Maeda, K.; Lu, D.; Domen, K. *ACS Catal.* **2013**, *3*, 1026−1033. Maeda, K.; Domen, K. *J. Catal.* **2014**, *310*, 67−74.

(7) Higashi, M.; Domen, K.; Abe, R. *J. Am. Chem. Soc.* **2013**, *135*, 10238−10241.

(8) Maeda, K.; Domen, K. *MRS Bull.* **2011**, *36*, 25−31.

(9) Kumagai, H.; Minegishi, T.; Moriya, Y.; Kubota, J.; Domen, K. *J. Phys. Chem. C* **2014**, *118*, 16386−16392.

(10) Liu, J.; Hisatomi, T.; Ma, G.; Iwanaga, A.; Minegishi, T.; Moriya, Y.; Katayama, M.; Kubota, J.; Domen, K. *Energy Environ. Sci.* **2014**, *7*, 2239−2242. Minegishi, T.; Nishimura, N.; Kubota, J.; Domen, K. *Chem. Sci.* **2013**, *4*, 1120−1124.

(11) Kanan, M. W.; Nocera, D. G. *Science* **2008**, *321*, 1072−1075.

(12) Moriya, M.; Minegishi, T.; Kumagai, H.; Katayama, M.; Kubota, J.; Domen, K. *J. Am. Chem. Soc.* **2013**, *135*, 3733−3735. Yokoyama, D.; Minegishi, T.; Jimbo, K.; Hisatomi, T.; Ma, G.; Katayama, M.; Kubota, J.; Katagiri, H.; Domen, K. *Appl. Phys. Express* **2010**, *3*, 101202. Yokoyama, D.; Minegishi, T.; Maeda, K.; Katayama, M.; Kubota, J.; Yamada, A.; Konagai, M.; Domen, K. *Electrochem. Commun.* **2010**, *12*, 851−853. Ma, G.; Minegishi, T.; Yokoyama, D.; Kubota, J.; Domen, K. *Chem. Phys. Lett.* **2011**, *501*, 619−622. Zhang, L.; Minegishi, T.; Kubota, J.; Domen, K. *Phys. Chem. Chem. Phys.* **2014**, *16*, 6167−6174. Zhao, J.; Minegishi, T.; Zhang, L.; Zhong, M.; Gunawan; Nakabayashi, M.; Ma, G.; Hisatomi, T.; Katayama, M.; Ikeda, S.; Shibata, N.; Yamada, T.; Domen, K. *Angew. Chem., Int. Ed.* **2014**, *53*, 11808.

(13) Paracchino, A.; Laporte, V.; Sivula, K.; Gratzel, M.; Thimsen, E. *Nat. Mater.* **2011**, *10*, 456−461.

DOI: 10.1021/ja5131879
J. Am. Chem. Soc. 2015, 137, 2227−2230